Evidence-based Preliminary Design of Spacecraft

6th International Conference on Systems & Concurrent Engineering for Space Applications

- SECESA 2014 -

08-10 October 2014

Vaihingen Campus, University of Stuttgart
Germany

Simone Alicino[(1)], Massimiliano Vasile[(1)]

[(1)]University of Strathclyde
75 Montrose Street, Glasgow, G1 1NW, Scotland
Email: simone.alicino@strath.ac.uk, massimiliano.vasile@strath.ac.uk

INTRODUCTION

In the design of a space system, contingency and margins based on historical data are used to cover for the unavoidable growth of resources such as mass, power, delta-V, propellant, cost, and others. In [1] contingency is defined as the difference between the current best estimate (BE) of a resource, or design budget, and its maximum expected value (ME), whereas margin is the difference between the maximum possible value (MP) and maximum expected value of the design budget, as shown in Fig. 1. Contingency accounts for expected growths due to uncertainties and variability, whereas margins account for unexpected ones due to unknown unknowns. Although based on historical data, and traditionally used, contingency does not give a rigorous quantification of the level of confidence the engineering team has on the best and maximum expected values of the design budget. A more rigorous approach is to quantify the uncertainties on the design variables and propagate them through the system model in order to obtain a quantification of the impact of the input and model uncertainties on the design budgets. For example, in Quantification of Margin and Uncertainty (QMU) [2], the ME is defined as best estimate plus uncertainty (BE+U), and is usually taken at 95-quantile of the cumulative distribution function (CDF) of the design budget; the current best estimate corresponds to another value of the cumulative distribution, and contingency can be determined, as shown in Fig. 2.
In preliminary systems engineering, uncertainties are usually epistemic, because they are due to imperfect or incomplete knowledge of some aspects of the system being designed. Indeed, as the design progresses, the level of knowledge increases and some assumptions made in the early phases are likely to be modified. Whereas in case of the aleatory uncertainties, i.e. due to inherent randomness of a physical phenomenon, probability theory can be effectively used to model the uncertain variables, in case of epistemic uncertainties the use of any probability distributions has been criticized, for they may not be representative of a phenomenon about which there is lack of knowledge. In this respect, imprecise probability theories can be a valuable tool. In particular, evidence theory is devised in such a way to conveniently capture epistemic uncertainty, and yet is similar enough to probability theory to approach it as the knowledge increases. In the framework of evidence theory, the level of confidence on a design parameter being in a certain interval/proposition is captured by a basic belief assigned to that interval/proposition. Once the uncertainties are propagated through the system model, evidence theory associates to the design budget two cumulative quantities, Belief (Bel) and Plausibility (Pl), that represent the level of confidence one has on the design budget being lower than that value. Therefore Belief and Plausibility are the evidence theory equivalent to the cumulative distribution function of probability theory, and indeed they can be seen as its lower and upper bounds, as shown in Fig. 2. For instance, the design budget for which the Belief is minimum (equals zero) is the most optimistic solution, whereas the design budget that maximizes it (equals one) is the worst-case scenario solution. The downside of an evidence-based approach is that the cost of computing Belief and Plausibility grows exponentially with the number of uncertain variables and intervals, as each focal element constituting the uncertain space needs to be evaluated and the number of focal elements results from the Cartesian product of the intervals of the uncertain variables.
This paper presents a computational tool that has been specifically developed for evidence-based robust design problems. The paper starts with a brief overview of evidence theory and its use in system design. Then a tool to reduce the computational cost of computing the Belief and Plausibility is discussed. The tool is composed of an evolutionary algorithm for worst-case scenario optimization, and a decomposition technique applicable to space systems engineering. Finally, a test case of the preliminary design of a small spacecraft will illustrate the results of the evidence-based robust design optimization in comparison to the margin approach.

EVIDENCE BASED DESIGN OPTIMIZATION

Evidence theory (also known as Dempster-Shafer theory)[3] belongs to a class of mathematical theories known as Imprecise Probabilities, which aim to generalize probability theory in those cases when no information on the

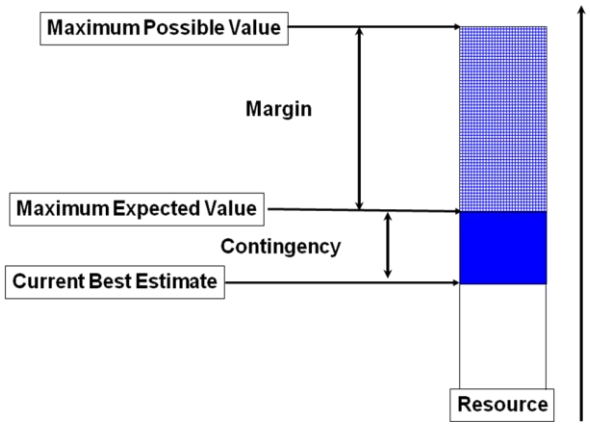

Fig. 1. Contingency and margin[1]

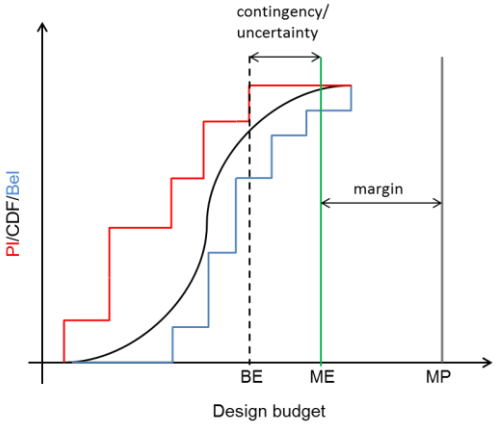

Fig. 2. Rigorous quantification of contingency

probability distributions is available. Therefore, it allows to adequately model both epistemic and aleatory uncertainty. The theory also provides a nice framework to incorporate multiple pieces of evidence in support to a interval/ proposition. For instance, during the preliminary design of an engineering system, experts can provide informed opinions by expressing their belief in an uncertain parameter u being within a certain set of intervals. The level of confidence an expert has in u belonging to one of the intervals is quantified by using a mass function generally known as Basic Belief Assignment (bba). An interval θ that has a non-zero bba is named a focal element. When more than one parameter is uncertain, the focal elements are the result of the Cartesian product of all the intervals associated to each uncertain parameter. The bba of a given focal element is then the product of the bba of all the intervals. The basic belief assignment $m(\theta)$ satisfies the axioms:

$$m(\theta) \geq 0, \forall \theta \in U; \quad m(\theta) = 0, \forall \theta \notin U; \quad m(\varnothing) = 0 \tag{1}$$

$$\sum_{\theta \in U} m(\theta) = 1 \tag{2}$$

All the pieces of evidence completely in support of a given proposition form the cumulative belief function Bel, whereas all the pieces of evidence partially in support of a given proposition form the cumulative plausibility function Pl. The Belief Bel and the Plausibility Pl functions are defined as follows:

$$Bel(A) = \sum_{\forall \theta_i \subseteq A} m(\theta_i) \tag{3}$$

$$Pl(A) = \sum_{\forall \theta_i \cap A \neq 0} m(\theta_i) \tag{4}$$

where A is the proposition about which Belief and Plausibility need to be evaluated. For example, the proposition can be expressed as:

$$A = \{u \in U \mid f(u) \leq \nu\} \tag{5}$$

where f is the outcome of the system model and the threshold ν is the desired value of a design budget (e.g. the mass). Thus, focal elements intercepting the set A, but not fully included in it, are considered in Pl but not in Bel. It is important to note that the set A can be disconnected or present holes, likewise the focal elements can be disconnected or partially overlapping.

COMPUTATIONAL APPROACH

Evidence theory is an interesting alternative in the preliminary design of an engineering system under uncertainty. An engineering system to be optimized can be modelled as a function f: $D \times U \subseteq \Re^{m+n} \rightarrow \Re$. The function f represents the model of the system budgets (e.g. power budget, mass budget, etc.), and depends on some uncertain parameters $u \in U$ and design parameters $d \in D$, where D is the available design space and U the uncertain space. What designers can be interested in is the maximum variation of the function f with u. In terms of Evidence theory, they are interested in the variation of the optimal Belief with the threshold ν. If q design budgets are to be concurrently optimized, then the following two problems can be solved without considering all the focal elements:

$$\mathbf{v}_{min} = \min_{\mathbf{d} \in D} [\min_{\mathbf{u} \in \bar{U}} f_1(\mathbf{d}, \mathbf{u}), \min_{\mathbf{u} \in \bar{U}} f_2(\mathbf{d}, \mathbf{u}), \ldots, \min_{\mathbf{u} \in \bar{U}} f_q(\mathbf{d}, \mathbf{u})] \tag{6}$$

$$\mathbf{v}_{max} = \min_{\mathbf{d} \in D} [\max_{\mathbf{u} \in \bar{U}} f_1(\mathbf{d}, \mathbf{u}), \max_{\mathbf{u} \in \bar{U}} f_2(\mathbf{d}, \mathbf{u}), \ldots, \max_{\mathbf{u} \in \bar{U}} f_q(\mathbf{d}, \mathbf{u})] \tag{7}$$

Problem (6) is a minimization over the design space D and the uncertain space $\bar{U}$, where $\bar{U}$ is a unit hypercube collecting all the focal elements in a compact set with no overlapping or holes. The transformation between U and $\bar{U}$ is

given by

$$\mathbf{x}_U = \frac{\left(\mathbf{b}^u_{U,i} - \mathbf{b}^l_{U,i}\right)}{\left(\mathbf{b}^u_{\bar{U},i} - \mathbf{b}^l_{\bar{U},i}\right)}\mathbf{x}_{\bar{U},i} + \mathbf{b}^l_{U,i} - \frac{\left(\mathbf{b}^u_{U,i} - \mathbf{b}^l_{U,i}\right)}{\left(\mathbf{b}^u_{\bar{U},i} - \mathbf{b}^l_{\bar{U},i}\right)}\mathbf{b}^l_{U,i} \tag{8}$$

where $\mathbf{b}^u_{U,i}$ and $\mathbf{b}^l_{U,i}$ (resp. $\mathbf{b}^u_{\bar{U},i}$ and $\mathbf{b}^l_{\bar{U},i}$) are the upper and lower boundaries of the i-th hypercube to which $\mathbf{x}_{U,i}$ (resp. $\mathbf{x}_{\bar{U},i}$) belongs. Problem (7) searches for the minimum of the maxima of all the functions over $\bar{U}$ and represents an example of worst-case scenario design optimization. The maximum (resp. minimum) of every function in (6), resp. (7), is independent of the other functions and corresponds to a different uncertain vector. Therefore, all the maxima (resp. minima) can be computed in parallel with q single-objective maximizations (resp. minimizations). The maximization (resp. minimization) of each function is performed by running a global optimization over $\bar{U}$.

In the single-objective case, (6) is solved by means of IDEA[4], a population-based memetic algorithm that hybridizes Differential Evolution and Monotonic Basin Hopping paradigms in order to improve local convergence capability, as demonstrated for some space trajectory optimization problems. Problem (7) is instead solved with IDEA𝒱[5], a variant of IDEA that implements a nested process where an outer loop minimizes f in the design space D, and for each $\mathbf{d}_i$ an inner loop maximizes f in the uncertain space U. In addition a series of cross-checks that evaluate f($\mathbf{d}_1$,$\mathbf{u}_2$) and f($\mathbf{d}_2$,$\mathbf{u}_1$) are necessary in order to increase the probability of maximizing the inner problem and correctly rank the solutions.

In the multi-objective case, (6) and (7) are solved by means of MACSminmax[6], an algorithm that makes use of a restoration procedure based on an iterative minimization over the design space and subsequent restoration of the global maximum over the uncertain space. The minimization is a multi-objective search performed by means of MACS2[7], a memetic algorithm for multi-objective optimization based on a combination of Pareto ranking and Tchebycheff scalarization. The maximization in the uncertain space is a single-objective search performed by means of IDEA.

Decomposition

Once the extremes $\boldsymbol{\nu}_{min}$ and $\boldsymbol{\nu}_{max}$ of Belief and Plausibility are computed, the full cumulative curves can be computed at a reduced cost by means of a decomposition technique. In the case of a system like a spacecraft, the mass of the system can be expressed as

$$f = \alpha_1\left(\mathbf{d}_1, \mathbf{u}_1, h_{\varphi_1}, ..., h_{\varphi_N}\right) + \alpha_2\left(\mathbf{d}_2, \mathbf{u}_2, h_{\varphi_1}, ..., h_{\varphi_N}\right) + \sum_{i=1}^{N} \varphi_i\left(\mathbf{d}_{\varphi_i}, \mathbf{u}_{\varphi_i}, h_{\varphi_i}(\mathbf{u}^h_{\varphi_i})\right) \tag{9}$$

where f is the total mass of the spacecraft, α_1 is the mass of the power subsystem, α_2 is the mass of the thermal subsystem, the φ_i are the masses of the other subsystems, and the coupling terms $h_{\varphi i}$ are the power consumptions of the subsystems, which indeed concur at sizing both power and thermal subsystems. In such a case the computation of Belief and Plausibility does not require the computation of all the focal elements. Indeed, Belief and Plausibility can be computed for each function α_i and φ_i, and then combined to find Belief and Plausibility of the overall function f. This would result in an exact computation if the functions α_i and φ_i were decoupled. If the functions are coupled, the result is an approximation of the real Belief and Plausibility. However, the coupling term can be sampled in order to obtain a more accurate approximation. The sampling of the coupling terms $h_{\varphi i}$ can be done as follows: for each function $h_{\varphi i}$ the Belief and Plausibility of the overall function f can be computed with respect of the uncertain vector $\mathbf{u}^h_{\varphi i}$ only, and fixing all the other design and uncertain variables to the solution of (7). Then, a number K_i of samples are taken for each $h_{\varphi i}$, and the focal elements of α_1, α_2, and φ_i are computed independently for each combination of samples and recombined to obtain an approximation Belief and Plausibility of f. The overall computational complexity becomes

$$n_{FE} = \prod_{i=1}^{N_\varphi} K_i \sum_{s=1}^{N_\alpha} \prod_{j=1}^{n_s} k_j + \sum_{i=1}^{N_\varphi}\left(K_i \prod_{j=1}^{n_i} k_{\varphi_j} + \prod_{j=1}^{n^h_i} k^h_{\varphi_j} \right) \tag{10}$$

where N_φ is the number of φ functions, N_α the number of α functions, n_s and k_j the number of uncertain variables and respective intervals for each alpha function, n_i and $k_{\varphi j}$ the number of uncertain variables and respective intervals for each φ function, and n^h_i and $k^h_{\varphi j}$ the number of uncertain variables and respective intervals for each $h_{\varphi i}$ function. Equation (10) shows that there is a significant reduction with respect to the exact computation of all the focal elements. For example, if one considers a function f with $N_\alpha = 2$, $n_s = 1$, $k_j = 3$, and $N_\varphi = 2$, $n_i = 1$, $k_{\varphi j} = 3$, $n^h_i = 2$ and $k^h_{\varphi j} = 3$, i.e. 8 uncertain variables in total, and each uncertain variables is composed of three intervals, the total number of focal elements is $3^8 = 6561$, corresponding to 13122 optimizations problems (one minimization and one maximization per focal element). By taking $K_i = 4$ samples for each h function, the number of focal elements to compute reduces to only 132, therefore about 2% of the total.

TEST CASE

In this section a test case is presented in which the methodology and computational tool described above are used to computed Belief and Plausibility of a simple small space system composed of attitude control, communications and power subsystems.

Attitude and Orbit Control Subsystem

The attitude and orbit control system (AOCS) is composed of the actuators that provide stability and orientation capability to the spacecraft. In the case of a small spacecraft in low Earth orbit and with 3-axis stabilization, the actuators are reaction wheels to provide stability against environmental disturbance torques, and magneto-torquers to unload the momentum stored in the wheels. The mass and power consumption of the AOCS are therefore

$$M_{AOCS} = M_{rw} + M_{mag} \tag{11}$$

$$P_{AOCS} = P_{rw} + P_{mag} \tag{12}$$

The total disturbance torque T_d on the spacecraft is the sum of solar pressure T_s, magnetic T_m, aerodynamic drag T_a, and gravity-gradient T_g torques. The solar pressure torque is

$$T_s = \frac{I_s}{c} Al(1+q) \tag{13}$$

where I_s is the incident solar radiation, c is the speed of light, A is the area of the spacecraft normal to the Sun, l is the offset between centre of gravity and centre of pressure of the satellite, and q is the reflectance factor. The magnetic torque is

$$T_m = m\frac{B_0 R_e^3}{(R_e + h)^3}\sqrt{3\sin^2(lat)+1} = mB \tag{14}$$

where m is the spacecraft residual dipole, B_0 is the planet's magnetic field strength, R_e is the planet radius, h is the altitude, lat is the magnetic latitude. The aerodynamic drag is

$$T_a = \frac{1}{2}\rho v^2 C_D Al \tag{15}$$

where ρ is the atmospheric density at the spacecraft altitude, v is the spacecraft velocity, C_D is the drag coefficient of the spacecraft, A is the area of the spacecraft normal to the velocity vector. The gravity gradient torque is

$$T_g = \frac{3\mu}{2(R_e + h)^3}\left|I_z - \min(I_x, I_y)\right|\sin(2\phi) \tag{16}$$

where μ is the planet gravitational parameter, I_z is the maximum moment of inertia of the satellite, and ϕ is the angle between the spacecraft z axis and the nadir vector. Typically, the moments of inertia are an epistemic uncertainty, therefore here an uncertainty factor δI is applied to I_x, I_y, and I_z. The momentum stored in the reaction wheels is

$$H_d = \frac{T_d P}{4e} \tag{17}$$

where P is the orbital period and e is the pointing accuracy. For an orientation, or slew, maneuvre, the momentum required is

$$H_{slew} = \frac{4\varphi_{slew} I_z}{t_{slew}} \tag{18}$$

where φ_{slew} is the slew angle, and t_{slew} is the time allowed for the maneuvre. The mass M_{rw} and power consumption P_{rw} of the reaction wheels can be computed by interpolating values[8] for real hardware with respect to the momentum required. For momentums of 0.0016, 0.4, 400 Nms, the masses are respectively 0.072, 2 and 20 kg, and the power consumptions are 0.465, 10 and 110 W. The bigger of H_d and H_{slew} sizes the reaction wheels. Magneto-torquers are used for momentum dumping of the reaction wheels. The magnetic dipole required can be computed as

$$D_{mag} = \frac{T_d}{B} \tag{19}$$

where B is specified in (13). The mass M_{mag} and power consumption P_{mag} of the magneto-torquer is computed by interpolating values for real hardware with respect to the momentum required. For dipoles of 0.06, 1, 4000 Am^2, the masses are respectively 0.0835, 0.4 and 50 kg, and the power consumptions are 0.155, 0.6 and 16 W.

Communications Subsystem

The telemetry and telecommand (TTC) system is composed of an antenna, a set of amplified transponders, and a radio frequency distribution network (RFDN). The mass of the TTC system is therefore the sum of the individual masses of the components

$$M_{TTC} = M_{ant} + M_{amp} + M_{rfdn} \tag{20}$$

The power required by the TTC system is

$$P_{TTC} = P_{amp} \tag{21}$$

Where P_{amp} is the power input required by the amplifiers, which depends on the transmitter power P_t that can be determined from the link equation

$$P_t = \frac{E_b}{N_0} - G_t - L_t - L_s - L_p - \frac{G_r}{T_s} + 10\log R - 228.6 \tag{22}$$

where E_b/N_0 is the ratio of received energy-per-bit to noise-density and is a function of frequency, modulation, coding, and required bit error rate (BER), which is usually set as a requirement. In this model the modulation is given as a design parameter, whereas the BER is given as a fixed parameter. The relationship between BER and E_b/N_0 is modelled for several modulations (such as PSK, BPSK, CFSK, BFSK, FSK, DPSK, QPSK and NRZ), and formulas can be found in [9]. The termo G_t is the transmit antenna gain, L_t is the onboard loss, L_s is the free space path loss, L_p is the propagation loss, G_r is the receive antenna gain, T_s is the system noise temperature, and R is the data rate.
The term G_r/T_s characterizes the receiving system, i.e. the ground segment, and is known for all the available ground stations. Because also the gain G_r is known, one can compute the nominal system noise temperature T_{s0},

$$T_{s0} = 10^{\frac{G_r - G_r/T_s}{10}} \tag{23}$$

The system noise temperature is affected by atmospheric conditions, as explained below.
The free space path loss L_s is caused by the distance between the two antennas, i.e. by increasing spherical surface area as radius increases

$$L_s = 92.44 + 20\log r + 20\log f \tag{24}$$

where r is the distance between the two antennas, in km, and f is the frequency in GHz.
The term L_p collects the propagation losses, such as atmospheric attenuation, rain attenuations, pointing loss, and other losses:

$$L_p = L_a + L_r + L_\theta + L_{other} \tag{25}$$

In the simplified model implemented in this paper, only atmospheric and rain attenuation and pointing loss have been modelled, whereas the term L_{other} collects all losses that have not been modelled. The atmospheric and rain attenuations depend on transmission frequency, elevation angle, altitude of the ground station. Moreover, a by-product atmospheric and rain attenuations is an increase in the system noise temperature T_{s0}

$$T_s = T_{s0} + T_{sa} + T_{sr} \tag{26}$$

where T_{sa} and T_{sr} are the contributions of atmpshpere and rain. Values for the losses L_a and L_r, as well as the noise temperatures T_{sa} and T_{sr}, can be estimated from tables provided by the International Telecommunication Union (ITU)[10].
The pointing loss L_θ can be estimated as [8]

$$L_\theta = -12\left(\frac{e}{\theta}\right)^2 \tag{27}$$

where e is the allowable pointing error, in deg, and θ is the half-power beamwidth, in deg.
The data rate R is computed as

$$R = \frac{V}{T_{ac}} \tag{28}$$

where V is the data volume, in bits, to be transmitted, and T_{ac} is the access time, in seconds, to the ground station.
The transmit antenna gain G_t is given as an input parameter, and permits to select and size the antenna. First, the antenna diameter D, in meters, and the half-power beamwidth θ, in degrees, are computed

$$D = \frac{\lambda}{\pi}\sqrt{\frac{G_t}{\eta_{ant}}} \tag{29}$$

$$\theta = 41253\frac{\eta_{ant}}{G_t} \tag{30}$$

The type of antenna is chosen basing on the gain: If $5 \le G_t \le 10$, a patch antenna is used; if $10 < G_t < 20$ a horn antenna is used; if $G_t \ge 20$ a parabolic dish is used.
For the patch antenna, the mass M_{ant} is determined as follows:

$$M_{ant} = \pi\frac{D^2}{4}\left(0.0005\rho_c + 0.0015\rho_d\right) \tag{31}$$

where ρ_c = 8940 kg/m^2 is the density of copper, whereas ρ_d = 2000 kg/m^2 is the density of the dielectric material.
The horn antenna is sized as follows. The lenght of the horn is computed as

$$l_{horn} = \sqrt{\frac{D^4}{9\lambda^2} - D^2/4} \tag{32}$$

The lateral surface area of the conic horn is then

$$S_{horn} = \frac{\pi D l_{horn}}{2} \tag{33}$$

and, finally, the mass of the horn antenna is

$$M_{ant} = S_{horn} \rho_{horn} \tag{34}$$

where ρ_{horn} is the surface density, here equal to 15 kg/m^2.
In case of parabolic antenna, Brown [11] provides a useful best fit formula for estimating the mass:

$$M_{ant} = 2.89 D^2 + 6.11 D - 2.59 \tag{35}$$

The mass M_{amp} and power input P_{amp} of the transponder can be estimated from data derived from actual flight hardware, as shown in [8]. Here we suppose that the transponder includes an amplifier that can be either a Traveling-Wave Tube Amplifier (TWTA) or a Solid-State Amplifier (SSA). The choice between the two types is a design trade-off. The mass M_{rfdn} of the remaining radio-frequency distribution network is here given as an input parameter.

Power Subsystem

The electrical power system (EPS) is composed of a solar array, a battery pack, a power conditioning and distribution unit (PCDU). The mass of the power system is the sum of the individual masses of the components

$$M_{EPS} = M_{sa} + M_{batt} + M_{pcdu} \tag{36}$$

The power produced by the system is the power converted by the solar array

$$P_{EPS} = P_{sa} \tag{37}$$

Given the power requirement P_n for the spacecraft night, as well as the duration t_n of the night, the energy capacity requirement of the battery system is

$$E_{req} = \frac{P_n t_n}{\eta_{b-l} DOD} \tag{38}$$

where η_{b-l} is the transfer efficiency between battery and loads, and is the product of the efficiencies of the battery discharge regulator, the distribution unit, and the harness

$$\eta_{b-l} = \eta_{bdr} \eta_{dist} \eta_{harn} \tag{39}$$

The efficiency η_{bdr} of the battery discharge regulator is a function of the bus voltage, and can assume values between 0.9 at 20 V and 0.97 at 100 V [9]. In case of unregulated bus, $\eta_{bdr} = 1$, as there is no discharge regulator. The harness efficiency η_{harn} is

$$\eta_{harn} = 1 - V_{drop}/100 \tag{40}$$

and is therefore dependent on the allowable voltage drop V_{drop} given as a percentage of the bus voltage. The efficiency of the distribution unit is $\eta_{dist} = 0.99$.
The depth of discharge DOD is function of the number CL of charge/discharge cycles, that is dependent on the orbit. Their relationship is estimated as [9]

$$DOD = -36.76 \ln \frac{CL}{207800} \tag{41}$$

Given the energy requirement for the battery, the mass of the battery pack is

$$M_{batt} = \frac{E_{req}}{E_{cell}} \tag{42}$$

where E_{cell} is the energy density (Wh/kg) of the cell, given in input. Finally, the charging efficiency η_{batt} of the battery is computed by interpolation of efficiencies [0.82, 0.83, 0.835, 0.95] and energy densities [37, 44, 51, 135] Wh/kg.
The power P_{sa} required from the solar array is computed from the power requirements P_d and P_n for the spacecraft daylight and night periods respectively, as well as the durations t_d and t_n of the periods

$$P_{sa} = \frac{P_n t_n}{\eta_{a-b} \eta_{b-l} t_d} + \frac{P_d}{\eta_{a-l}} \tag{43}$$

where η_{a-b} is the transfer efficiency between solar array and battery pack, η_{a-l} is the transfer efficiency between solar array and loads. The power requirements are a typical epistemic uncertainty in preliminary design, therefore an uncertainty factor δP is applied to P_d and P_n. The transfer efficiencies can be expressed as the product of the efficiencies of the components:

$$\eta_{a-b} = \eta_{sar} \eta_{bcr} \eta_{batt} \tag{44}$$

$$\eta_{a-l} = \eta_{sar} \eta_{dist} \eta_{harn} \tag{45}$$

where η_{bcr} is the efficiency of the battery charge regulator and, as for the discharge regulator, can assume values between 0.9 at 20 V and 0.97 at 100 V, or 1 if the bus is unregulated, and η_{sar} is the efficiency of the solar array

regulator, and assumes values between 0.94 at 20 V and 0.99 at 100 V for direct energy transfer (DET) configuration, or between 0.93 at 20 V and 0.97 at 100 V for maximum power peak tracking (MPPT) configuration.
Solar cells suffer from several factors that decrease their efficiency. Increasing the temperature of the cell reduces the power generated by the cell. At a certain temperature T, the change in efficiency is given by

$$\eta_{\text{temp}} = 1 - \eta_{\text{T}}\left(\text{T} - \text{T}_{\text{nom}}\right) \tag{46}$$

where η_{T} is the degradation per centigrade, which assumes values between 0.005 for cell efficiency of 0.16, and 0.002 for cell efficiency of 0.28, and T_{nom} is the nominal temperature of the solar cell, usually 28°C. Several other factors concur at degrading the efficiency of the solar cell. The array pointing loss factor is

$$\eta_{\text{p}} = \cos\alpha \tag{47}$$

where α is the solar incidence angle. The distance r_{S} (in AU) from the Sun involves a loss, or gain, that is

$$\eta_{\text{r}} = \frac{1}{\text{r}_{\text{S}}^{2}}. \tag{48}$$

Furthermore, cells degrade with time mainly due to radiation fluence, and such degradation can be estimated as in [8]

$$\eta_{\text{life}} = \left(1 - \text{D}_{\text{cell}}\right)^{\text{life}}. \tag{49}$$

where D_{cell} is the cell degradation per year, and life is the cell life time. A further important factor affecting the efficiency of the solar array is the assembly efficiency η_{a}. The efficiency of the array is lower than the efficiency of the single cells because of a loss due to assembly. Such factor is usually uncertain and is given as input. The total cell efficiency is therefore $\eta_{\text{tot}} = \eta_{\text{a}}\eta_{\text{temp}}\eta_{\text{p}}\eta_{\text{r}}\eta_{\text{life}}$. The specific power ($\text{Wh/m}^2$) of the array is

$$\text{P}_{\text{cell}} = 1370\eta_{\text{cell}}\eta_{\text{tot}} \tag{50}$$

From this, the required area of the array is computed

$$\text{A}_{\text{sa}} = \frac{\text{P}_{\text{sa}}}{\text{P}_{\text{cell}}} \tag{51}$$

and finally the mass of the solar array

$$\text{M}_{\text{sa}} = \text{A}_{\text{sa}}\rho_{\text{sa}} \tag{52}$$

where ρ_{sa} is the specific mass of the solar array, in kg/m^2.
The PCDU is a modular unit composed of modules such as battery charge and discharge regulators, solar array regulators, maximum power point tracker, shunt regulator, distribution unit (latching current limiters), telemetry interface. The number of modules, and therefore the mass of the unit, is dependent on the power system configuration. Indeed, if the bus is unregulated, there are no battery charge and discharege regulators, therefore the PCDU is lighter. If the configuration is DET, there is no maximum power point tracker, and the PCDU is lighter. On the other hand, an MPPT configuration extract maximum power from the solar array, therefore the array size decreases, but the presence of the MPPT module decreases the transfer efficiency and increases the PCDU mass. The configuration is a typical trade-off in the design, and is a design parameter. The mass Mpcdu can be estimated as the sum

$$\text{M}_{\text{pcdu}} = \mu_{\text{pcdu}}\left(2\text{P}_{\text{sa}} + \text{bP}_{\text{d}} + \text{bP}_{\text{e}} + \text{cP}_{\text{sa}}\right) \tag{53}$$

where $\mu_{\text{pcdu}} = 0.001$ kg/W, b is the bus type (0 for unregulated, 1 for regulated bus), c is the configuration (0 for DET, 1 for MPPT), and the 2 multiplying the first term in brackets accounts for a telemetry and a distribution unit.

RESULTS

Tables 1 to 3 collect the values of the design, uncertain, and fixed parameters for the subsystems discussed above. For the design parameters a range is specified as well as a nominal value (bolded). The uncertain parameters are usually quantified in terms best-case, worst-case, and nominal (or most likely, bolded) values, that can be nicely translated into quantifications in the framework of Evidence theory.
The model is composed of 10 design parameters and 16 uncertain parameters. Each uncertain parameter has two intervals, therefore there is a total of 65536 focal elements. Fig. 3 shows the Belief and Plausibility curves computed by means of the decomposition method with $\text{K}_{\text{i}} = 3$, together with the actual curves, for comparison. One can see that the Belief curve is estimated with very good accuracy by taking only 3 samples per h function, that is by evaluating only 374 focal elements, the 0.57% of the total. The Plausibility is instead underestimated. The best case solution (Pl = 0) is $\nu_{\text{min}} = 1.19$ kg, whereas the best worst-case solution (Bel = 1) is $\nu_{\text{max}} = 1.82$ kg. In Fig. 3 also the best estimate is shown, corresponding to the nominal values of the design and uncertain parameters. One can see that the BE, 1.62 kg, corresponds to a Belief of 0.4 and a Plausibility of 1. This means that, with the current quantification of the uncertainty, one can state that the confidence in the nominal solution is between 40% and 100%. In addition, if one takes as maximum expected value the mass corresponding to a Belief of 1, the contingency can be calculated rigorously, and it is 11%. Note that a further margin might be still applied to cover for unexpected growths.
A further use of the Evidence-based design could be in making informed decisions on margin policies at subsystem level, as contingencies can be computed rigorously for each subsystem separately. For example, Figg. 4 to 6 show Belief and Plausibility, along with the BE value for each subsystem individually. Once again, one can see the upper and

lower bounds of the confidence level, and quantify rigorously the contingencies, with respect to mass value corresponding to Bel = 1, at subsystem level. For example the optimal contingencies for AOCS, TTC, and EPS are respectively 3.5%, 21.3% and 8.3%. Therefore an optimal margin policy can be tailored based on the uncertainty associated to each subsystem.

Table 1. Design parameters

AOCS		TTC		EPS	
φ_{slew}, deg	[10 60] **(10)**	f, GHz	[7 10] **(8.253)**	η_{cell}	[0.15 0.30] **(0.28)**
t_{slew}, s	[30 90] **(90)**	modulation	[0 1] **(1)**	E_{cell}, Wh	[135 145] **(145)**
		amplifier	[TWT SSP] **(SSP)**	V_{bus}, V	[3 5] **(5)**
				V_{drop}, %	[1 3] **(1)**
				configuration	[DET MPPT] **(MPPT)**

Table 2. Uncertain parameters

AOCS			TTC			EPS		
l, m	[0.005 **0.01**] bba 0.5	[0.01 0.02] bba 0.5	η_{ant}	[0.6 **0.8**] bba 0.3	[0.8 0.9] bba 0.8	D_{cell}	[0.025 **0.0275**] bba 0.8	[0.03 0.0375] bba 0.2
A, m^2	[0.034 **0.0885**] bba 0.5	[0.0885 0.15] bba 0.5	G_t, dB	[1 **3**] bba 0.3	[3 5] bba 0.7	η_a	[0.8 **0.85**] bba 0.4	[0.85 0.9] bba 0.6
q	[0. 5 **0.6**] bba 0.5	[0.6 0.7] bba 0.5	L_t, dB	[0.1 **0.5**] bba 0.3	[0.5 1.0] bba 0.7	ρ_{sa}, kg/m^2	[3.5 **3.6**] bba 0.5	[3.6 4.0] bba 0.5
m, mA·m^2	[0.5 **1**] bba 0.5	[1 1.5] bba 0.5	L_{other}, dB	[0.5 1.5] bba 0.4	[1.5 **2.0**] bba 0.6	δP, %	[0 **10**] bba 0.3	[10 20] bba 0.7
C_D	[2.0 **2.2**] bba 0.5	[2.2 2.5] bba 0.5	M_{rfdn}, kg	[0.1 **0.3**] bba 0.4	[0.2 0.5] bba 0.6	T_{max}, C	[0 **10**] bba 0.4	[10 15] bba 0.6
δI, %	[-10 5] bba 0.4	[5 **10**] bba 0.6						

Table 3. Fixed parameters

AOCS		TTC		EPS	
P, s	5850	BER	1e-5	P_d, W	$16 + P_{TTC} + P_{AOCS}$
B_0, T	3.1e-5	V, bits	1e6	P_n, W	$16 + P_{TTC} + P_{AOCS}$
I_s, W/m^2	1420	G_r/T_s, dB/K	30	t_d, h	1.615
lat, deg	80	h, km	640	t_n, h	0.0103
μ, km^3/s^2	398600	el, deg	10	r_S, AU	1
ϕ, deg	5	e, deg	5	α, deg	5
v, km/s	7.54	G_r, dB	60	life, years	1
R_e, km	6378	T_{ac}, s	600	bus regulation	regulated
I_x, kg·m^2	0.0417			CL	14250
I_y, kg·m^2	0.1083				
I_z, kg·m^2	0.1417				

CONCLUSIONS

In this paper we presented an approach for rigorous quantification of contingency and uncertainty that is applicable to preliminary design. Evidence theory provides a useful framework to treat both epistemic and aleatory uncertainty, but has a computational cost that grows exponentially with the number of uncertain variables and intervals. A tool is then presented that substantially reduces such cost by first finding the best and worst-case scenarios, and then using a decomposition technique to find an approximation of the full cumulative Belief and Plausibility functions. A test case composed of three subsystems of a spacecraft has shown how the methodology can be effectively applied to a real case. The Belief and Plausibility could be computed with acceptable accuracy at a fraction of the computational expense. This allows for a rigorous quantification of the contingency the engineering team should account for in preliminary design.

ACKNOWLEDGMENT

The authors wish to thank Quirien Wijnands of ESA/ESTEC for his support and help in the development and validation of the subsystem models. This work is partially supported through an ESA/NPI grant 'Evidence-based Robust Design Optimization'.

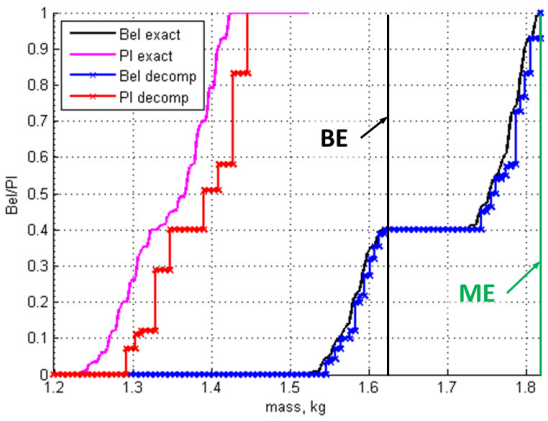

Fig. 3. Belief, Plausibility, best estimate and maximum expected value of the spacecraft mass

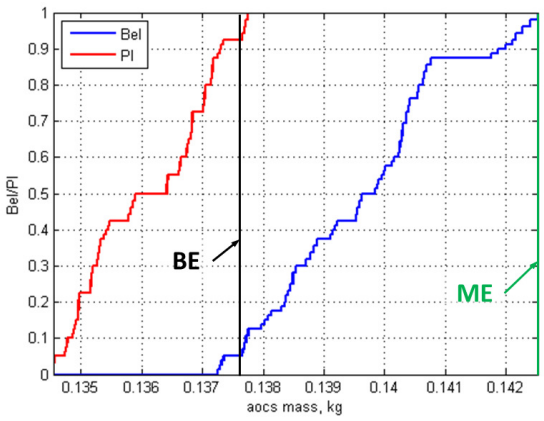

Fig. 4. Belief, Plausibility, best estimate and maximum expected value of the AOCS mass

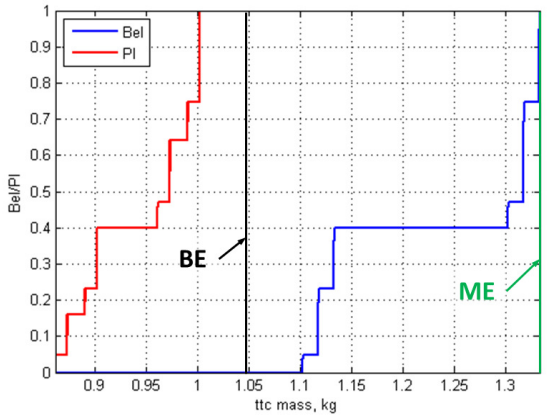

Fig. 5. Belief, Plausibility, best estimate and maximum expected value of the TTC mass

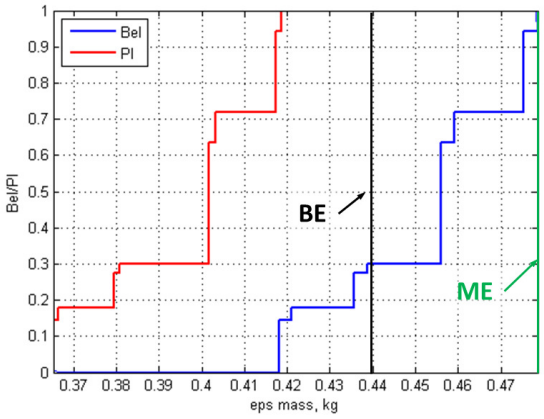

Fig. 6. Belief, Plausibility, best estimate and maximum expected value of the EPS mass

REFERENCES

[1] AIAA Standard, "Mass Properties Control for Space Systems," S-120-2006e, 2006.

[2] M. Pilch, T.G. Trucano and J.C Helton, "Ideas Underlying Quantification of Margins and Uncertainties (QMU): A White Paper", Tech. Rep. SAND2006-5001, Sandia National Laboratories, September 2006.

[3] G. Shafer, A Mathematical Theory of Evidence, Princeton University Press, 1976.

[4] M. Vasile, E. Minisci and M. Locatelli, "An Inflationary Differential Evolution Algorithm for Space Trajectory Optimization," IEEE Trans Evol Comp. vol. 15, pp. 267-281, April 2011.

[5] M. Vasile and E. Minisci, "An Evolutionary Approach to Evidence-Based Multidisciplinary Robust Design Optimisation," Evolutionary and Deterministic Methods for Design Optimization and Control, 2011.

[6] S. Alicino and M. Vasile, "Analysis of Two Algorithms for Multi-Objective Min-Max Optimization," 6th International Conference on Bioinspired Optimization Methods and their Application, September 2014.

[7] F. Zuiani and M. Vasile, "Multi Agent Collaborative Search Based on Tchebycheff Decomposition", Comput. Optim. Appl., vol. 56, pp. 189-208, 2013.

[8] J.R. Wertz and W.J. Larson, Space Mission Analysis and Design, 3rd ed., Microcosm Press, 1999.

[9] W. Ley, K. Wittmann and W. Hallmann, Handbook of Space Technology, John Wiley & Sons Ltd, 2009.

[10] Attenuation by Atmospheric Gases, Rec. ITU-R P.676-9, 2012.

[11] C.D. Brown, Elements of Spacecraft Design, AIAA Education Series, 2002.